

# A DIY Bioreactor for in Situ Metabolic Tracking in 3D Cell Models via Hyperpolarized $^{13}\text{C}$ NMR Spectroscopy

Lluís Mangas-Florencio,<sup>¶</sup> Alba Herrero-Gómez,<sup>¶</sup> James Eills, Marc Azagra, Marina Batlló-Rius, and Irene Marco-Rius\*



Cite This: *Anal. Chem.* 2025, 97, 1594–1602



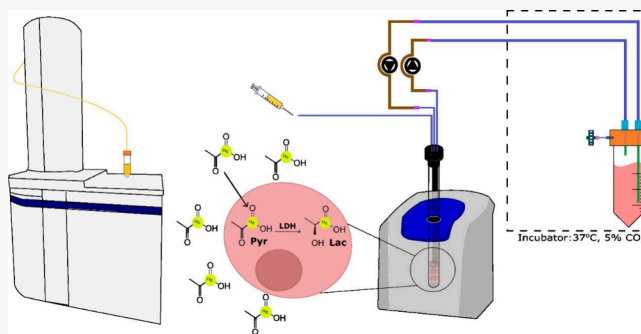
Read Online

ACCESS |

Metrics & More

Article Recommendations

**ABSTRACT:** Nuclear magnetic resonance (NMR) spectroscopy is a valuable diagnostic tool limited by low sensitivity due to low nuclear spin polarization. Hyperpolarization techniques, such as dissolution dynamic nuclear polarization, significantly enhance sensitivity, enabling real-time tracking of cellular metabolism. However, traditional high-field NMR systems and bioreactor platforms pose challenges, including the need for specialized equipment and fixed sample volumes. This study introduces a scalable, 3D-printed bioreactor platform compatible with low-field NMR spectrometers, designed to accommodate bioengineered 3D cell models. The bioreactor is fabricated using biocompatible materials and features a microfluidic system for media recirculation, ensuring optimal culture conditions during NMR acquisition and cell maintenance. We characterized the NMR compatibility of the bioreactor components and confirmed minimal signal distortion. The bioreactor's efficacy was validated using HeLa and HepG2 cells, demonstrating prolonged cell viability and enhanced metabolic activity in 3D cultures compared to 2D cultures. Hyperpolarized [ $1\text{-}^{13}\text{C}$ ] pyruvate experiments revealed distinct metabolic profiles for the two cell types, highlighting the bioreactor's ability to discern metabolic profiles among samples. Our results indicate that the bioreactor platform supports the maintenance and analysis of 3D cell models in NMR studies, offering a versatile and accessible tool for metabolic and biochemical research in tissue engineering. This platform bridges the gap between advanced cellular models and NMR spectroscopy, providing a robust framework for future applications in nonspecialized laboratories. The design files for the 3D printed components are shared within the text for easy download and customization, promoting their use and adaptation for further applications.



## INTRODUCTION

Nuclear magnetic resonance (NMR) spectroscopy is an outstanding diagnostic tool in clinical settings. However, NMR is hampered by low sensitivity due to the low net nuclear spin polarization of the samples analyzed. In recent years, hyperpolarization (HP) techniques such as dissolution dynamic nuclear polarization (dDNP) have been used to increase nuclear spin polarization in chemicals and materials by >10,000-fold, giving a corresponding enhancement in the observable signal intensity, reducing analysis time.<sup>1</sup> As an example, this enhancement allows for the tracking of energy metabolism and its products in real time, providing deeper molecular insight into cellular processes unmatched by alternative tools that are limited to quantification of metabolite uptake, such as PET.<sup>2</sup>

Another limitation of high resolution NMR is that the magnetic field needs to be homogeneous, which typically requires the use of glass NMR tubes and small sample volumes. This is incompatible with the correct culture conditions for current bioengineered cellular models, so specialized NMR-

compatible bioreactors have been designed for use in cellular applications. In the last years, bioreactor (BR) platforms have been used to advance the field of HP-NMR data acquisition to record cellular metabolism in real-time.<sup>3,4</sup> However, to excel in their application, most of these platforms are designed to fit a fixed NMR tube diameter such as 5 mm,<sup>5,6</sup> 10 mm,<sup>7–9</sup> or 20 mm,<sup>10</sup> limiting their translation for use in instruments with different magnet bores.

The previously described BRs are fabricated and tested to be analyzed in high field NMR spectrometers.<sup>5,11–13</sup> The limited widespread application of NMR in bioengineering and other biological laboratories is partly due to the need for a superconductive magnet and spectrometer, which are speci-

**Received:** August 7, 2024

**Revised:** January 8, 2025

**Accepted:** January 9, 2025

**Published:** January 15, 2025



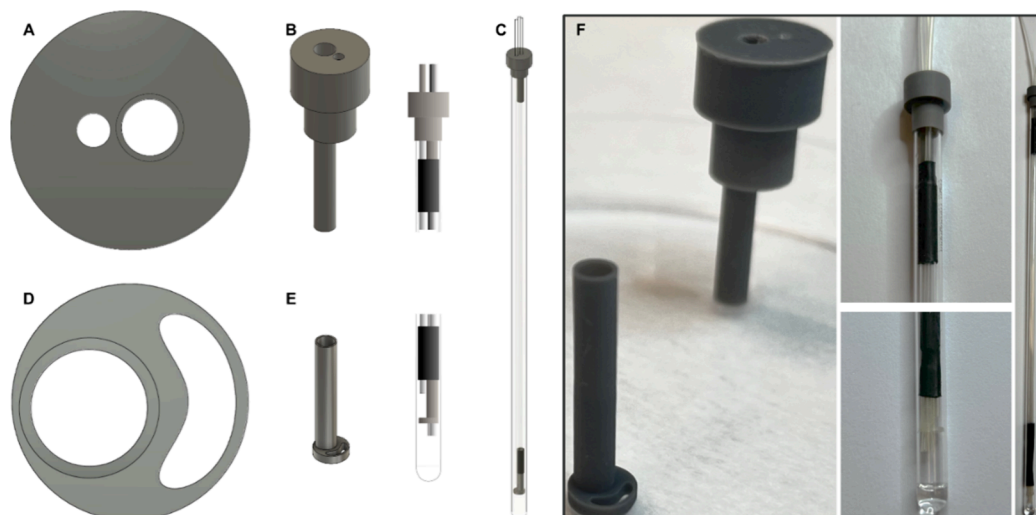


**Figure 1.** Bioreactor design: 3D renderings of the custom cap piece (A, B), stopper (D, E) and schematic of their assembly in an NMR tube (C). (F) Photos showing the individual components and their assembly.

alized pieces of equipment not typically found in standard bioengineering facilities. This requirement makes NMR and BRs less accessible, restricting their use to well-equipped research institutions. Cryogen-free benchtop NMR systems, on the other hand, offer a viable solution for nonspecialized research facilities, providing more accessible and affordable options for integrating NMR technology into a broader range of laboratories. Furthermore, the experimental displays presented in previous publications require complex set-ups with probes, sensors, and automated control systems,<sup>6,8,14</sup> making them somewhat inaccessible to nonspecialized NMR laboratories. Moreover, most BR designs are customized to host specific cellular models, such as cells encapsulated in collagen, alginate or polystyrene microcarrier beads.<sup>10,13,15</sup> While the high specificity in their design greatly enhances their performance in particular applications,<sup>16</sup> it further decreases their versatility when measuring biological samples with different spatial and cell media availability requirements such as organoids or scaffolded 3D cell models.

Here we present a new bioreactor design for benchtop NMR systems. The units are designed to be 3D printed and scalable to the desired NMR tube diameter, and the platform can be adjusted depending on the height and dimensions of the detection area of the instrument. The materials of the platform and media circulation system are biocompatible, and the perfusion circuit allows for cell maintenance inside the bioreactor before, during and even after the experiment. Moreover, by adjusting the platform and the components' distribution in the NMR tube, the bioreactor can be scaled to different spectrometers and adjusted to fit different biological samples and their individual cell culture needs.

As the field of tissue engineering evolves, researchers worldwide have described biologically advanced cell constructs with specific mechanical properties, dimensions, and biological requirements for optimal and unbiased analysis.<sup>17–19</sup> By limiting the culture space in the NMR tube and including a microfluidic system for media recirculation, we aim to optimize acquisitions keeping the sample in the detection area of the spectrometer throughout the experiment. For HP applications that require a quick injection of a probe through the sample, most of the BR perfusion systems previously described use a single inlet tube for HP substrate and media.<sup>5,20,21</sup> In this

design, a separate injection microfluidic system is used, which makes it easy to remove the channel from the design and simplify the bioreactor if the application being considered does not require it. Having a separate HP channel helps ensure hyperpolarized substrate removal from the microfluidic system after injection by minimizing its interaction with new cell media, thus reestablishing optimal cell media conditions for subsequent culture and longitudinal studies. The design originates from the need for an easily accessible and customizable bioreactor platform to make NMR an available tool to investigate cellular biochemical processes for other NMR and non-NMR-specialized laboratories.

After careful study of the design and its assembly, we tested two different human cell models in the bioreactor and characterized the flow conditions in the detection area, the viability of the cells after the HP substrate perfusion, and their survival after manipulation inside and outside the NMR tube. These characterizations were performed both with and without the BR platform, mimicking the cell stress induced when placing the models inside an NMR tube without a media support system to reduce the time outside optimal cell culture conditions. After characterizing the circulation system, we tested its effectiveness during HP-NMR experiments and its accuracy detecting differences in cellular metabolism between two cancerous cell types using an astonishingly low (>10 times lower) number of cells when compared to previously described bioreactors.<sup>13,15,20</sup> Moreover, we tested the accuracy of the BR platform to differentiate between the metabolism produced by both cancerous cell types, either in suspension or bioengineered into 3D cell models. These experiments highlight the relevance of the spatial distribution of the cells under study depending on each application, having an impact on the metabolic data obtained.

## EXPERIMENTAL SECTION

All NMR experiments were conducted on a 1.4 T Pulsar Benchtop Spectrometer with a 5 mm bore at 37 °C (Oxford Instruments, Oxford, UK).

**Development of MR-Compatible Bioreactor Design and Fabrication of Custom Components.** The individual components of the bioreactor were designed using AutoCAD

(Autodesk Inc.) and Fusion 360 (Autodesk Inc.) CAD software. The BR consists of three custom parts and 5 standard components. An individual view of the parts can be seen in Figure 1. Table 1 provides a description for both custom and standard parts, manufacturers and commercial references.

**Table 1. Bioreactor Components**

Description	Manufacturer	Commercial ref.	Part of
Bioreactor cap	Custom	–	Bioreactor
Bioreactor stopper	Custom	–	Bioreactor
PDMS spacer	Custom	–	Bioreactor
3 mm ID glass tube	Norell	NORS38007	Bioreactor
0.51 mm ID silicone tubes	Freudenberg medical	45630102	Bioreactor
0.76 mm ID silicone tubes	Freudenberg medical	45630104	Fluidic system
Metallic connectors	Darwin microfluidics	AE-20G-100x	Fluidic system
Peristaltic pump	Heidolph Instruments	523-52010-00	Fluidic system

The bioreactor cap and stopper were fabricated using a 3D printer in a cleanroom environment. The 3D design<sup>22</sup> was exported to MicroForm (MicroRay SLA Systems, ES) and printed on a MicroRay Versus 385 nm 3D Printer (MicroRay SLA Systems, ES). The biocompatible translucent Freeprint Ortho (DETAX, DE) resin was used for the stopper piece and the opaque resin solus Art Gray V3.0 (Junction3D, USA) for the bioreactor cap. To create the polydimethylsiloxane (PDMS) spacer at the bottom of the tube, the polymeric base was mixed with the curing agent (Sylgard 184, Dow Corning, USA) in a ratio of 10:1 (w/w). The mixture was carefully introduced in the 5 mm NMR tube without leaving residue on the walls and the PDMS was cured vertically leveled overnight at 60 °C for a uniform surface.

Three silicone tubes (0.51 mm ID, 0.94 mm OD) constitute the microfluidic system inside the BR. All three of the channels go through the BR cap, and the HP injection and media entry channels cross through the BR stopper piece and terminate in the culture space. To give structure and stability, the silicone tubing is sheathed in a short glass section of 3 mm OD NMR tube. All the pieces were joined to the bioreactor custom parts with heat shrink tubes for a tight fit.

The bioreactor was connected to the peristaltic pump (Hei-Flow, Heidolph Instruments, Schwabach, DE) using metallic connectors and 0.76 mm ID silicone tubing. The system was closed after connection to a reservoir to hold the cell media and ensure free exchange of CO<sub>2</sub> in the incubator through a 0.22 mm filter in the reservoir. The system was tested to withstand up to 1 mL/min media flow and fast injection through the HP channel, however the cell experiments were performed with 0.2 mL/min cell media flow to mimic physiological conditions and reduce shear stress.

**Characterization of NMR Compatibility and Signal Interference.** To design a reliable BR platform, it was imperative to characterize the benchtop NMR spectrometer used and the position of its RF coil. The precise position of the RF coil in the benchtop NMR spectrometer was determined to within 1 mm precision in separate experiments, to allow the bioreactor samples to be correctly positioned and guide the assembly of the BR.

To determine the degree of NMR signal distortion caused by the bioreactor materials, an NMR tube with 10% H<sub>2</sub>O in D<sub>2</sub>O (v/v) was prepared. Pure H<sub>2</sub>O would give an artificially broadened NMR resonance due to radiation damping,<sup>23</sup> which would obscure our search for small signal distortions from the bioreactor components. The different pieces of the BR were added one by one to an NMR tube in their correct position and the spectral fwhm was analyzed after the addition of each component. To verify the results, the experiment was performed using two different methods. First, the reference fwhm was measured after shimming the spectrometer with the 90% D<sub>2</sub>O sample and before adding any part of the bioreactor. Different parts of the bioreactor platform were added in turn, and <sup>1</sup>H NMR spectra were acquired of the 10% H<sub>2</sub>O sample. In a second set of experiments, the benchtop magnet was shimmed after the addition of each BR piece and before <sup>1</sup>H NMR signal acquisition.

**Biomaterial Preparation for 3D Cell Model.** Carboxymethyl cellulose (CMC) scaffolds were fabricated as described in previous publications.<sup>24,25</sup> All materials used for the fabrication were purchased from Sigma-Aldrich.

Briefly, 1% CMC (w/v) was diluted in Milli-Q water under stirring. A cross-linker mixture containing 0.5 M 2-ethanesulfonic acid (MES) buffer at 5.5 pH from MES hydrate, 50 mg/mL adipic acid dihydrazide (AAD), and 1 μg/μL N-(3-(dimethylamino)propyl)-N'-ethylcarbodiimide hydrochloride (EDC) all dissolved in Milli-Q water and vortexed until homogeneity, was added to the fully dissolved 1% CMC solution. The final prepolymer solution contained 1 mL of 1% CMC dilution, 50 mM of MES buffer, 1.83 mM AAD, and 18.9 μM EDC. The solution was vigorously mixed with a pipet to avoid early cross-linking while obtaining a homogeneous mixture. For fluorescein-stained cryogels, 10.9 μM of fluoresceinamine were added to the final solution before polymerization.

The solution was swiftly transferred into PDMS annular cylinder molds with 2 mm height and 10 mm diameter over a cover glass. The filled molds were covered with a glass sheet and placed at –20 °C overnight. For demolding and shaping, the cryogels were submerged in phosphate buffered saline (PBS) and cut into 5 mm diameter discs using a 5 mm biopsy punch. The cryogels were moved into fresh PBS and autoclaved for further cell seeding.

**Cell Culture and 3D Cell Modeling.** To assess accuracy when measuring cell metabolism in two distinct human cell lines, both HeLa and HepG2 cells were used. HeLa human adenocarcinoma cells were cultured in Dulbecco's modified Eagle's medium (DMEM) with 4.5 g/L glucose (Gibco, ThermoFisher), 10% fetal bovine serum (FBS) (Gibco, ThermoFisher) and 1% penicillin-streptomycin (P/S) (10<sup>4</sup> U/mL) (ThermoFisher Scientific, ES). HepG2 human hepatoblastoma cells (CliniSciences, USA) were cultured in Eagle's Minimum Essential Medium (EMEM) (ATCC, 30-2003) supplemented with 10% FBS and 1% P/S (10<sup>4</sup> U/mL).

Cells were grown in T175 cm<sup>2</sup> flasks and incubated at 37 °C in a 5% CO<sub>2</sub> humidified atmosphere. Cell media was changed every 48–72 h as required. Once the cells reached 80% confluence, the culture vessel was washed once with PBS, cells were detached using Trypsin-EDTA (0.25%) solution and centrifuged (200 g, 3 min). The supernatant was discarded, and the pellet was resuspended in complete growth media at a density of 10<sup>8</sup> cells/mL for seeding onto the scaffolds.

The cells were seeded onto the scaffolds as previously described.<sup>25</sup> The cryogels were lined up in 12 well plates and 10  $\mu\text{L}$  of cell suspension ( $10^6$  cells) were seeded in each scaffold. The plate was introduced in the incubator, and 2 mL of growth media were added after 20 min. Twenty-four h after seeding, the cryogels were moved into a new plate and cell medium of the cryogels was replaced every 48 h in culture.

**Cell Viability Assay.** Cell viability was assessed with metabolic alamarBlue (aB) HS assay (ThermoFisher Scientific, ES) and confocal imaging (LSM 800 Leica, ZEISS Iberia). This metabolic test was used to calculate cellular activity inside the scaffolds at days 2, 4, 7, 9, and 11.

The aB assay of the 3D models was performed in 96 well plates, where each cell-laden scaffold was placed in a well with 90  $\mu\text{L}$  of medium and 10  $\mu\text{L}$  of reagent. To compare the scaffolded cells with traditional monolayer cell culture,  $0.5 \times 10^5$  cells were seeded in each well of a 6-well plate the same day the cell-laden scaffolds were assembled, allowing for parallel tests with the 3D models. For 2D aB experiments, 900  $\mu\text{L}$  of medium and 100  $\mu\text{L}$  of reagent were placed in each well. The plates were incubated for 1 h and analyzed in a microplate reader (Infinite M200 PRO, Tecan) with 560 nm excitation and 590 nm emission filters.

Furthermore, cell-laden scaffolds were imaged using the LSM 800 Leica scanning laser confocal microscope operating with ZEN 2.3 (blue edition) imaging software to assess cell viability, distribution and aggregation of the scaffolded cells. Using live cell dyes, dead cells were stained with Propidium Iodide (PI) (Sigma-Aldrich, DE), Hoechst 33342 (ThermoFisher Scientific, ES) was used to mark the cell nucleus as a counterstain, and ViaFluor 488 (Biotium, USA) was used to identify the microtubules of the cytoskeleton. The cell-laden cryogels were washed three times with sterile PBS for 5 min to remove all cell media from the constructs. Afterward the cell-laden scaffolds were stained in a PBS solution containing 3  $\mu\text{M}$  PI, 1 mg/mL Hoechst 33342, and 1 mg/mL ViaFluor 488. The cryogels were incubated for 30 min and the excess dye was washed with PBS. After washing, the cryogels were set in the PDMS molds mounted on a microscope slide. The molds were filled with fresh sterile PBS and covered with a coverslip for imaging.

**Assessment of Culture Conditions and Manipulation Strain in the BR Setup.** To assess the capability of the BR as a culture vessel, the metabolic activity of the cell-laden scaffolds under flow conditions was assessed through aB assay, using the protocol described above. Briefly, a 3D cell model was placed in the BR with the circulation system connected to a reservoir filled with fresh cell media inside the incubator at culture conditions (37  $^\circ\text{C}$  and 5%  $\text{CO}_2$ ), with a peristaltic pump connecting both the reservoir and the bioreactor with a 0.2 mL/min media flow recirculation. The 3D models were maintained with continuous flow in the BR for 24 h, after which they underwent an aB assay to assess their viability. As control group, 3D-laden scaffolds were placed inside a 5 mm NMR tube with 400  $\mu\text{L}$  of fresh growth media without the recirculation system for 24 h to mimic long acquisition times without a BR platform for media renewal.

In addition, we conducted tests to assess the metabolic status of the scaffolded cells following the HP-NMR experimental procedure, specifically evaluating cell viability. This assessment aimed to validate the biological suitability of the platform, taking into account any stress induced on the cells through manipulation. The cell-laden scaffolds were

loaded into the NMR tube either with or without the BR platform, then nonhyperpolarized pyruvate (leftover from previous hyperpolarized pyruvate experiments) mixed with cell media at 37  $^\circ\text{C}$  to obtain a solution with final pyruvate concentration of 3.2 mM. 1 mL of the mixture was injected simulating the experimental HP-NMR procedure. Following injection, we tested the biological relevance of a recirculation system to reestablish optimal culture conditions in the 3D cell models. Five minutes after pyruvate injection, to account for standard HP-NMR data acquisition, the media recirculation in the bioreactor group was restarted. The first 3 mL of media exiting the BR were purged to quickly infuse the BR with fresh growth medium, reestablishing optimal culture conditions. Thirty minutes after injection, all 3D cell models were studied with the aB assay to determine the impact of media recirculation on cell viability immediately after injection.

**BR Accuracy Detecting Different Cellular Metabolism through HP-NMR.** For HP  $^{13}\text{C}$  NMR experiments,  $2 \times 10^6$  scaffolded cells in the BR were placed inside the benchtop spectrometer at 37  $^\circ\text{C}$  prior to the experiment. Immediately prior to the HP substrate injection, the media recirculation system was stopped for the acquisition and resumed promptly afterward to restore the system to optimal pyruvate concentrations. Via confocal imaging, there were no observable differences in cell conformation inside scaffolds prior and post HP-NMR experiments.

For HP  $^{13}\text{C}$  pyruvate preparation, HP [ $^{13}\text{C}$ ]pyruvic acid was prepared by adding 15 mM of OX063 radical (GE Healthcare) and 1.5 mM Dotarem (Guerbet S.A., FR) to neat [ $^{13}\text{C}$ ]pyruvic acid (99%  $^{13}\text{C}$  enriched, Sigma-Aldrich Isotec, Miamisburg, OH). The mixture was polarized at 1.4 K in a 3.5 T magnetic field using a commercial dissolution-DNP polarizer HyperSense (Oxford Instruments, UK) via 45 min of positive-lobe microwave irradiation at 94,155 GHz and with 100 mW of microwave power. After polarization, the cryogenic samples were dissolved in 4.5 mL of a heated phosphate buffered saline solution supplemented with 1% HEPES, 0.01% EDTA, 0.1% NaCl, and 0.2% NaOH and ejected from the instrument at 37  $^\circ\text{C}$ . After dissolution, HP [ $^{13}\text{C}$ ]pyruvate was further diluted with growth media. One mL of this solution containing 3.2 mM HP [ $^{13}\text{C}$ ]pyruvate was injected into the bioreactor through the injection port. The  $^{13}\text{C}$  NMR spectra were acquired dynamically with a train of 15 $^\circ$  flip angle pulses with a pulse repetition time of 5 s for a total of 200 s.

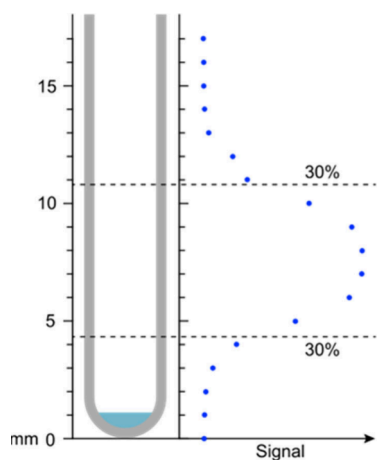
**Data Analysis.** Statistical analysis was performed using GraphPad Prism 9.2.0. Results are expressed as mean  $\pm$  standard deviation. One-way ANOVA or student's *t* test with a *p*-value of  $<0.05$  were used to assess significant differences between groups.

For analysis of the HP  $^{13}\text{C}$  NMR experiments, a custom software in MATLAB (The MathWorks, USA) was employed. First, data preprocessing, including line broadening of 1 Hz, zero-filling, baseline correction and phase correction was applied across all spectra. Next, spectra for each experiment were aggregated, and automatic peak detection was performed. The area under the curve (AUC) of  $^{13}\text{C}$ -lactate and  $^{13}\text{C}$ -pyruvate peaks was then computed using automatically defined integration regions. The  $^{13}\text{C}$ -lactate/ $^{13}\text{C}$ -pyruvate ratio was then determined by dividing the respective AUCs. Signal-to-noise ratio (SNR) of all peaks was also calculated. Experiments with  $^{13}\text{C}$ -lactate peaks with a SNR less than 7 were excluded to minimize the influence of significant noise contributions.

## RESULTS AND DISCUSSION

**Design, Fabrication and Assembly of the Bioreactor Platform.** A new BR platform has been designed and tested for the metabolic and biochemical study of tissue engineered 3D cell models with NMR. First, the design was conceived with its versatility in mind, allowing for easy customization to adjust the dimensions as needed for each application. We provide the files of the 3D printed pieces so that it can be readily reproduced by others.<sup>22</sup>

The versatility of the 3D custom pieces suggests the potential for scaling when using 10 or 20 mm NMR tubes, though testing the new BR configuration would be needed before its use. The assembly process favors the adjustability of the platform to different heights, effectively tailoring to each NMR spectrometer's detection area. The characterization of the detection area of the 1.4 T Pulsar benchtop spectrometer determined the detection region to start 4.5 mm from the bottom of the NMR tube. Figure 2 presents a schematic representation of the coil position determined by the intensity of the <sup>1</sup>H NMR signal. Consequently, the PDMS piece was designed to be 4.5 mm in height.



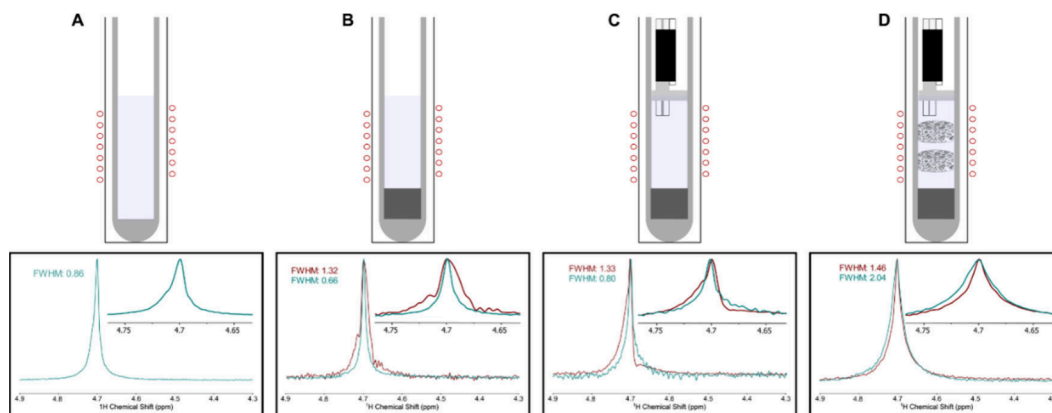
**Figure 2.** Detection area characterization in the 1.4 T NMR benchtop Pulsar instrument. Schematic representation of the maximum detection region in an NMR tube determined by <sup>1</sup>H NMR water analysis.

Figure 1 shows the bioreactor design where the custom cap piece (Figure 1A,B) allows the microfluidic tubes to reach the cell chamber for effective media recirculation and HP-substrate injection. The stopper piece (Figure 1D,E), together with the PDMS spacer at the bottom, maintained the cell chamber fit to the detection area, reducing technical variability between experiments.

**Bioreactor NMR Line Shape Analysis.** After characterizing the coil position and dimensions of the detection area in the spectrometer, the measurements of the BR components were adjusted to fit the cell chamber to the detection area of the instrument. The compatibility of the BR materials with NMR acquisitions was studied for each piece in close proximity to the detection area. In Figure 3 we show a comparison between the lineshapes of the unshimmed and shimmed samples, in red and blue, respectively. After using two different experimental approaches to characterize possible signal distortions, the fwhm values for all acquisitions proved similar ( $1.21 \pm 0.44$ ) without any significant distortions detected.

NMR line shape analysis experiments showed that the presence of the bioreactor components near the detection area does not significantly impact the NMR line widths. This poses advantages, such as simplifying experimental processes by reducing adjustments, as there is no need to do a secondary shimming after preparing the BR setup. The 1% CMC scaffold was characterized for its NMR properties and it was determined to be non-NMR active. Additionally, its demonstrated diffusion properties<sup>26</sup> make it a suitable construct for both NMR and HP-NMR metabolic studies.

**Bioreactor Suitability for Culture of 3D Cell Models.** We then assessed the biocompatibility of the bioreactor platform. First, we assessed the biocompatibility of the 1% CMC scaffolds, which must allow for easy cell seeding and act as a suitable host for the 3D cell models. After seeding the cells in the scaffolds and incubating them overnight, the cells self-arranged in clusters (Figure 4C), with a homogeneous but random cell distribution observed through the 3D construct. Moreover, no dead cells were detected with confocal imaging in the clusters, neither after seeding nor subsequent culture up to 11 days. This poses a significant increase in viability when compared to the traditional monolayer cultures (Figure 4D). Furthermore, the confocal images confirm minimal cell death



**Figure 3.** Validation of the bioreactor NMR compatibility. The <sup>1</sup>H NMR spectra of the 10% H<sub>2</sub>O in D<sub>2</sub>O samples are shown in either blue (shimming after the addition of each BR component) or red (only shimming at the beginning of the experiment before adding any BR components). The four variations tested were: (A) NMR tube (no bioreactor components). (B) PDMS spacer. (C) PDMS spacer and bioreactor stopper. (D) PDMS spacer, bioreactor stopper, and two CMC-scaffolds (i.e., all components of the bioreactor in the NMR-active region).

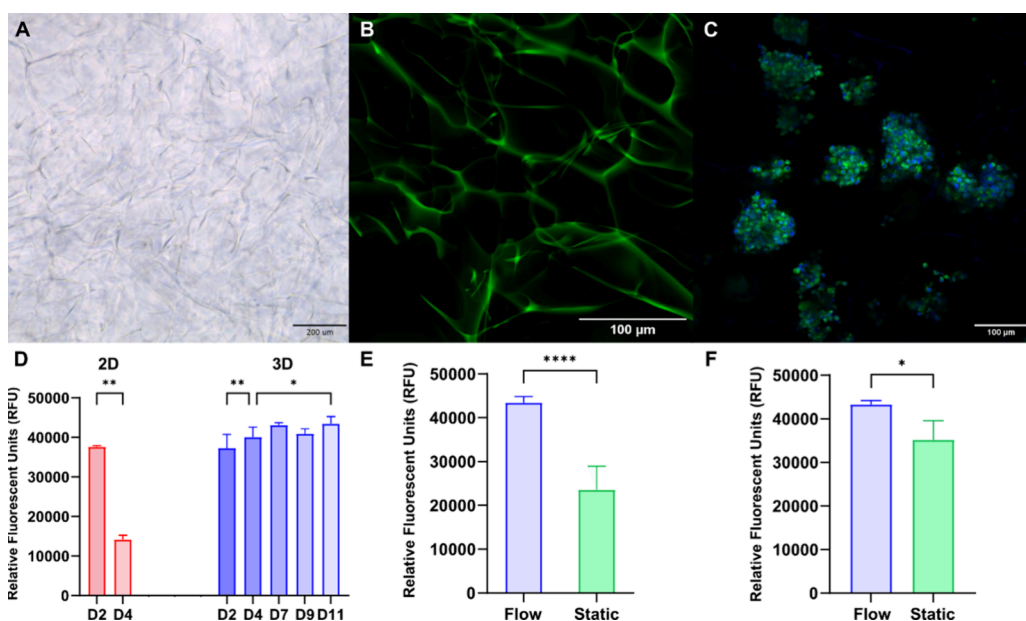


**Figure 4.** Validation of the 3D cell model and bioreactor recirculation system. (A) Structure of the cryogel through brightfield optical microscopy. (B) Structure of the cryogel through microscope confocal imaging of the fluoresceinamine stained cryogels. (C) HeLa cell clusters self-assembled in the cryogel after seeding as seen through confocal imaging. Nuclei in blue (Hoechst 33342), cytoskeleton microtubules in green (ViaFluor 488) and apoptotic cells in red (Propidium Iodide). (D) Metabolic activity of HeLa cells cultured in 2D (in a plate) or 3D (in a CMC scaffold) for up to 11 days, measured using alamarBlue. (E) Metabolic viability of the 3D constructs assessed using alamarBlue after 20 h with and without media recirculation in the BR or NMR tube, respectively. (F) Metabolic activity of the cell-laden scaffolds 1 h after injection of non-HP pyruvate solution, with and without flow in the BR. Data are normalized to cell number at the time of seeding and are presented as mean  $\pm$  SD of at least three independent experiments.

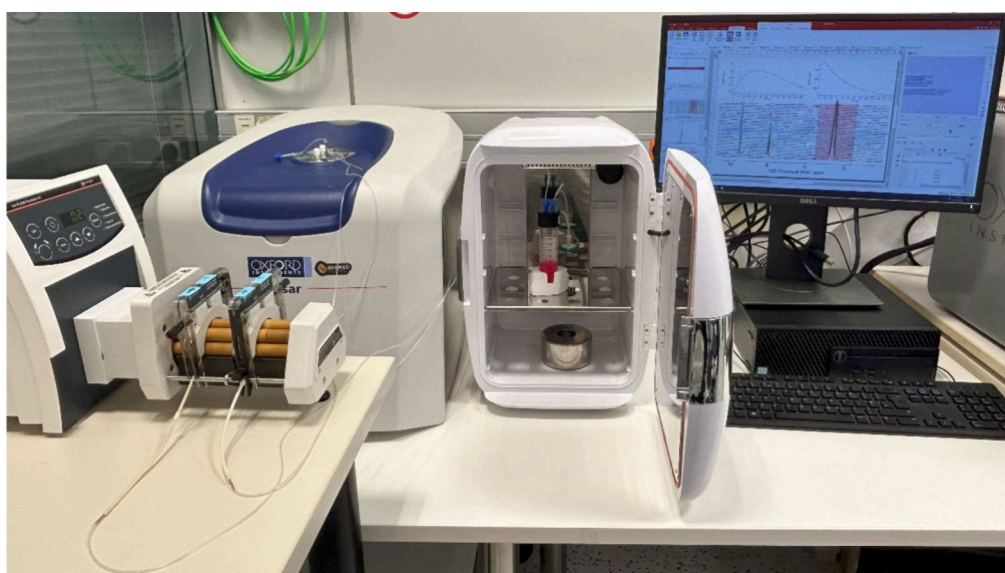


**Figure 5.** Picture of the setup used for 3D cell construct experiments. The BR containing the 3D cell model was placed inside the 1.4 T benchtop and connected to a reservoir of fresh cell media at culture conditions inside and incubator. The peristaltic pump at 0.2 mL/min was used for media recirculation between the reservoir and the BR.

among the clusters, suggesting that the promotion of cell–cell interactions in the 3D cell conformation allows the cells to be maintained in viable conditions for up to 11 days.

This effect is also evident in the results obtained from the aB assays performed, with a significant decrease in cell metabolism between day 2 and 4 in 2D cells (average decrease of 62.5%), illustrating a decrease in viability. A significant difference in metabolic activity can also be observed between day 2 and day 4 in 3D cell cultures, with an average increase of 7.45%, and

between day 4 and 11 (average increase of 8.4%). This tendency is expected as the literature suggests that cells arranged in 3D conformation demonstrate reduced proliferative rates when compared to their 2D counterparts.<sup>27–29</sup> The results of the aB assays further illustrate the advantages that 3D cell cultures present to create robust and reliable cell models, allowing samples to be further cultured and reanalyzed if necessary.

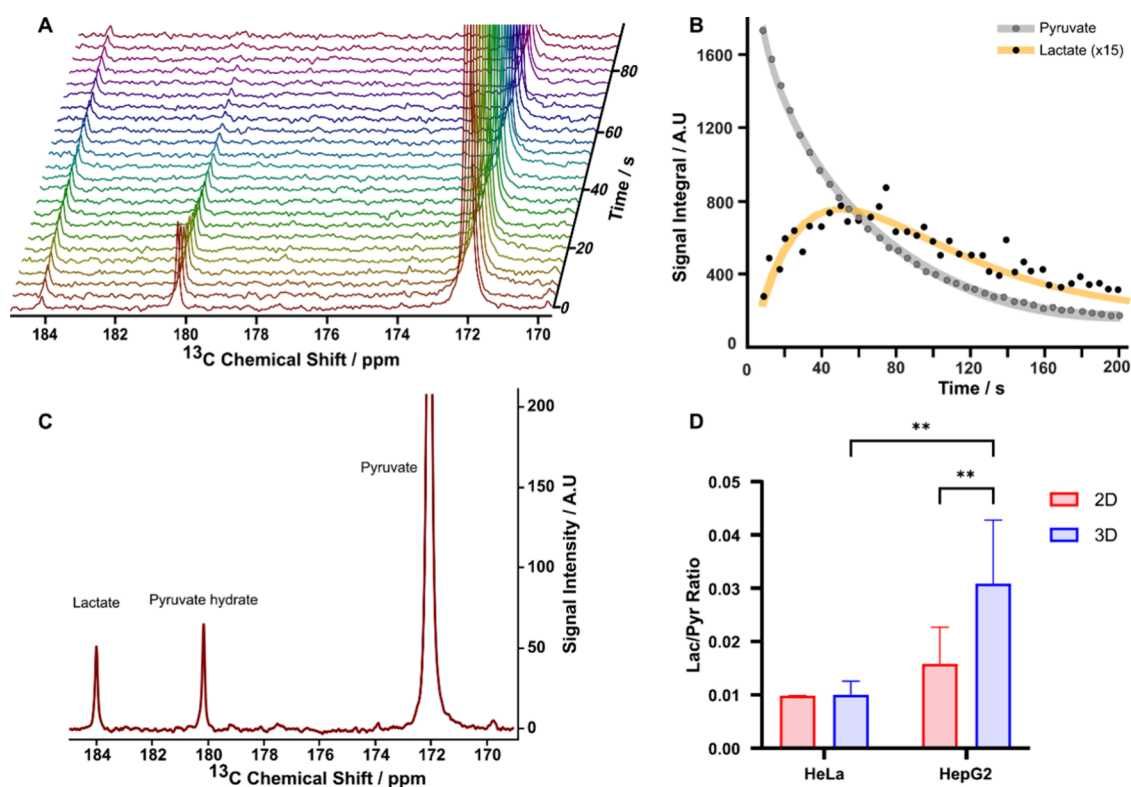


**Figure 6.** Metabolic study in the bioreactor of HeLa and HepG2 cell models. (A) Representative dynamically acquired  $^{13}\text{C}$  NMR spectra of HepG2-laden 3D scaffolds every 5 s after injection of hyperpolarized pyruvate solution. (B) Plot of the integral values of the pyruvate and lactate signals from the  $^{13}\text{C}$  NMR spectra of a single experiment over time. (C) Sum-up of the dynamic spectra containing metabolic data presented in panel A. The SNR on the  $^{13}\text{C}$  pyruvate resonance was 750:1. (D) Calculated lactate-to-pyruvate ratios obtained from the sum-up spectra for either HeLa 2D and 3D models ( $N = 3$  and  $5$  respectively) or HepG2 2D and 3D models ( $N = 10$  and  $5$  respectively). Data are presented as mean  $\pm$  SD.

Furthermore, the efficiency of the media recirculation system was examined to assess the suitability of the BR as a cell culture platform. After placing the cell models in an NMR tube either with or without the BR setup (Figure 5), the microfluidic system was started at a flow of 0.2 mL/min and both groups were left overnight in the incubator. As seen in Figure 4E, the viability of the 3D cell models that were kept without media recirculation decreased by 45.73% in average, while the 3D cell models maintained with the BR platform maintained their viability. Confocal imaging further confirmed this data, as no dead cells could be observed in the clusters after being in the BR with the media recirculation system for 20 h.

Additionally, the need for media renewal after injection of a HP substrate was demonstrated using nonhyperpolarized  $^{13}\text{C}$  pyruvate. The cell models were placed in the BR, injected with a nonpolarized pyruvate solution, and either left in the static mixture of pyruvate solution and cell media, or the media recirculation system was restarted to provide fresh media. After 30 min, the 3D cell models that had no recirculation and were left in the static pyruvate/media solution displayed an average decrease in cell viability of 18.7% compared to samples with media recirculation (Figure 4F). The data presented includes at least three independent experiments for each condition with three replicates each.

When characterizing its biocompatibility, we see that 3D cell cultures in the bioreactor retain their viability under cell media flow, and cell viability is not affected by hyperpolarized or traditional NMR acquisitions.

### Using the BR to Contrast Metabolism between Different Cell Models.

To validate the bioreactor platform for HP-NMR analysis, we carried out experiments both on 2D and 3D cell cultures in the bioreactor in a 1.4 T benchtop NMR magnet. For these experiments, we injected 1 mL of 3.2 mM hyperpolarized [ $1\text{-}^{13}\text{C}$ ] pyruvate solution into the bioreactor, and tracked the metabolic conversion of HP  $^{13}\text{C}$ -pyruvate (172 ppm) into HP  $^{13}\text{C}$ -lactate (184 ppm) over 200 s using  $^{13}\text{C}$  NMR. We carried out experiments using two different epithelial cell types: adenocarcinoma cells (HeLa) and hepatoblastoma cells (HepG2), to test the accuracy of the platform to discern between different metabolic profiles. We also carried out experiments on 2D cell cultures to further characterize the impact on data variability when choosing a 3D cell model over a traditional monolayer culture for metabolic studies. For the 2D experiments the cells were lifted from their culture flask immediately prior to the dissolution and counted using trypan blue exclusion stain. Then,  $2 \times 10^6$  cells were transferred into a 5 mm NMR tube for metabolic analysis using common protocols previously described for these types of studies.<sup>30</sup> For the experiments with the 3D cell models, the cell-laden scaffolds were transferred into the BR platform for analysis minutes before the HP shot. The dynamic  $^{13}\text{C}$  NMR experiments allowed us to detect the change in HP  $^{13}\text{C}$ -pyruvate and  $^{13}\text{C}$ -lactate signals over time (Figure 6A). In Figure 6B we plot the integrals of the pyruvate and lactate peaks over time to show the pyruvate signal decay (due to relaxation and conversion to lactate), and the lactate signal build-up and subsequent decay (due to the competition between production from pyruvate and relaxation).

Since increased lactate production is correlated with cell activity, to quantify the metabolic activity of the cells we summed up the individual spectra containing metabolic products and took the ratio between the pyruvate and lactate peak integrals. An example sum-up spectrum is shown in Figure 6C. For these experiments, the 2D cells were trypsinized, and either 2D cells or 3D cell constructs were placed in the BR for testing. After placing the loaded BR in the benchtop spectrometer and subsequent  $1\text{-}^{13}\text{C}$ -pyruvate injection, spectra were dynamically acquired every 5 s. All experimental conditions were tested in replicates, with each replicate using a fresh cell sample to ensure reliable comparison across different conditions. We observe significant differences between the metabolic profiles for the different cells and culture conditions (2D vs 3D). While HeLa cells show no significant metabolic differences between 2D cell suspensions and 3D conformation, HepG2 cells portray a significantly different metabolic profile when engineered in 3D constructs compared to the metabolic data obtained in 2D cell suspensions (Figure 6D). The HepG2 cells in the 3D cell model showed a 2.2-fold higher rate of lactate production compared to their 2D counterparts.

The results of this study align with the need to develop better biocompatible NMR platforms for metabolic and biochemical studies of tissue engineered models. With NMR providing valuable insight on the molecular composition of cells and their metabolic status, new BR platforms help bridge the gap between NMR and tissue engineering. Optimizing the culture conditions inside an NMR tube, the BR can be used to study a myriad of 3D cell constructs, adjusting the models to the detection area of the spectrometer for robust data acquisition. This adjustment allows to maximize signal detection by ensuring that all metabolic products are produced within the detection area. Consequently, sample size can be reduced when compared to previous studies<sup>7,13</sup> without hampering data acquisition, effectively reducing the number of cells required to detect metabolism in real time via HP-NMR. This improvement opens the door for NMR to be implemented as a characterization tool for highly specialized models that are oftentimes constituted by fewer cells.<sup>15</sup> Furthermore, the BR can be used to maintain and study these 3D models over time, capitalizing on the nondestructive nature of NMR spectroscopy, especially attractive for 3D cell models that are scarce and technically difficult to develop.

Nonetheless, this study has limitations, including the assumption that the BR would be as effective as reported for higher hierarchy biological models, including complex matrices, multiple cell types, or spatial constraints that might affect media and HP substrate distribution through the model. Even so, the versatility of the BR design allows for easy addition of features to cater to these specific needs; acknowledging that all cell models tested with the BR hereby described should first undergo characterization to detect any design changes needed for each application. Furthermore, the temperature of the platform is controlled directly by the internal heating of the spectrometer, which for this study was set and characterized at 37 °C. However, if the spectrometer used does not include this feature, the cell media should be lightly heated over 37 °C and the media recirculation system shortened and insulated to reduce heat loss and maintain the cell model inside a physiological temperature range. Such solutions have been previously reported with more complex bioreactor setups.<sup>12,31</sup>

## CONCLUSIONS

While the concept of an NMR bioreactor is not novel, and the setups previously described excelled at their application<sup>5,21,32</sup> their versatility is reduced by their design and the distribution of the space allocated to the cell models analyzed. As shown in this study, the conformation of the cells and their spatial distribution has an impact on the metabolic data obtained. This aligns with the belief in tissue engineering that certain cell models and cell types ought to be studied in 3D conformation to better mimic native physiology and produce biologically relevant metabolic data.<sup>33,34</sup> Therefore, providing an NMR-compatible analytical platform such as a BR, makes NMR more accessible as a tool to study and characterize the biochemical environment in these novel 3D cell models. In this work we show the first example of an NMR bioreactor designed for use in benchtop NMR systems, which are more accessible for nonspecialized laboratories. Overall, our work is a step to bridge the gap between tissue engineering and NMR, making the technology available to researchers looking to obtain molecular data on their cell models while only having access to low-field NMR spectrometers.

## ASSOCIATED CONTENT

### Data Availability Statement

All research data are available from the corresponding author upon request. The 3D designs of the bioreactor developed for this research are available in the CORA public depository at [10.34810/data1540](https://doi.org/10.34810/data1540).

## AUTHOR INFORMATION

### Corresponding Author

Irene Marco-Rius – *Institute for Bioengineering of Catalonia (IBEC), Barcelona Institute of Science and Technology (BIST), 08028 Barcelona, Spain*; [orcid.org/0000-0001-5076-8526](https://orcid.org/0000-0001-5076-8526); Email: [imarco@ibecbarcelona.eu](mailto:imarco@ibecbarcelona.eu)

### Authors

Lluís Mangas-Florencio – *Institute for Bioengineering of Catalonia (IBEC), Barcelona Institute of Science and Technology (BIST), 08028 Barcelona, Spain*; *Vitala Technologies, S.L., 08028 Barcelona, Spain*; *University of Barcelona, 08028 Barcelona, Spain*; [orcid.org/0000-0003-1306-6351](https://orcid.org/0000-0003-1306-6351)

Alba Herrero-Gómez – *Institute for Bioengineering of Catalonia (IBEC), Barcelona Institute of Science and Technology (BIST), 08028 Barcelona, Spain*; *University of Barcelona, 08028 Barcelona, Spain*; [orcid.org/0000-0002-8807-0649](https://orcid.org/0000-0002-8807-0649)

James Eills – *Institute for Bioengineering of Catalonia (IBEC), Barcelona Institute of Science and Technology (BIST), 08028 Barcelona, Spain*; [orcid.org/0000-0001-8468-6860](https://orcid.org/0000-0001-8468-6860)

Marc Azagra – *Institute for Bioengineering of Catalonia (IBEC), Barcelona Institute of Science and Technology (BIST), 08028 Barcelona, Spain*

Marina Batlló-Rius – *Vitala Technologies, S.L., 08028 Barcelona, Spain*

Complete contact information is available at:

<https://pubs.acs.org/10.1021/acs.analchem.4c04183>

### Author Contributions

<sup>¶</sup>L.M.-F. and A.H.-G. contributed equally to this work. L.M.-F. coded and performed the experiments, data acquisition

and processing, and cowrote the manuscript. A.H.G. co designed and performed the experiments, data acquisition, and cowrote the manuscript. J.E. performed NMR experiments, analyzed the data, and reviewed the manuscript. M.A. performed NMR experiments, analyzed the data, and reviewed the manuscript. M.B.R. analyzed the data and reviewed the manuscript. I.M.R. initiated the project, reviewed the manuscript, raised funding and supervised the work.

## Notes

The authors declare the following competing financial interest(s): I.M.R. is co-founder and CSO of Vitala Technologies S. L. The authors declare that they have no other competing interests.

## ACKNOWLEDGMENTS

We thank Dr. Alejandro Portela and Dr. Jose L. Muñoz for experimental help, Francesc Subirada and Dr. Josep Samitier for their technical support, and the MicroFabSpace and Microscopy Characterization Facility, Unit 7 of ICTS 'NANBIOSIS' from CIBER-BBN at IBEC for their support. LMF received financial support through the MCIN/AEI/DIN2021-012097. AHG received financial support from the FI Fellowship Programme from AGAUR (ref. 2021 FI\_B\_01039). J.E. received funding from the European Union's Horizon 2020 Research and Innovation Programme under the Marie Skłodowska-Curie Grant Agreement 101063517. This work is part of a project that has received funding from the Junior Leader Postdoctoral Fellowship Programme from "la Caixa" Banking Foundation (LCF/BQ/PI18/11630020), the European Union's Horizon 2020 research and innovation program (GA-863037), the BIST – 'la Caixa' initiative in Chemical Biology (CHEMBIO). MCIN/AEI/10.13039/501100011033 (ref. PID2020-117859RA-I00), MCIN/AEI/10.13039/501100011033 and "ESF Investing in your future" (ref. RYC2020-029099-1), MICIU/AEI/10.13039/501100011033 and "ERDF/EU" (ref. PID2023-151470OB-I00), MCIN/AEI/10.13039/501100011033 and by the "European Union NextGenerationEU/PRTR" (ref. PLEC2022-009256).

## REFERENCES

- (1) Adamson, E. B.; Ludwig, K. D.; Mummy, D. G.; Fain, S. B. *Phys. Med. Biol.* **2017**, *62*, R81–R123.
- (2) Rohren, E. M.; Turkington, T. G.; Coleman, R. E. *Radiology* **2004**, *231*, 305–332.
- (3) Gaspar, D.; Gomide, V.; Monteiro, F. *The role of perfusion bioreactors in bone tissue engineering*. 2012.
- (4) Wolfe, S. P.; Hsu, E.; Reid, L. M.; Macdonald, J. M. *Biotechnol. Bioeng.* **2002**, *77*, 83–90.
- (5) Keshari, K. R.; Wilson, D. M.; Van Criekinge, M.; Sriram, R.; Koelsch, B. L.; Wang, Z. J.; VanBrocklin, H.; Peehl, D. M.; O'Brien, T.; Sampath, D.; et al. *Physiology behavior* **2017**, *176*, 139–148.
- (6) Sriram, R.; Van Criekinge, M.; Hansen, A.; Wang, Z. J.; Vigneron, D. B.; Wilson, D. M.; Keshari, K. R.; Kurhanewicz, J. *NMR in Biomedicine* **2015**, *28*, 1141–1149.
- (7) Keshari, K. R.; Sriram, R.; Koelsch, B. L.; Van Criekinge, M.; Wilson, D. M.; Kurhanewicz, J.; Wang, Z. J. *Cancer research* **2013**, *73*, 529–538.
- (8) Radoul, M.; Najac, C.; Viswanath, P.; Mukherjee, J.; Kelly, M.; Gillespie, A. M.; Chaumeil, M. M.; Eriksson, P.; Delos Santos, R.; Pieper, R. O.; Ronen, S. M. *NMR in Biomedicine* **2019**, *32*, 1–23.
- (9) Witney, T. H.; Kettunen, M. I.; Hu, D. E.; Gallagher, F. A.; Bohndiek, S. E.; Napoli-tano, R.; Brindle, K. M. *Br. J. Cancer* **2010**, *103*, 1400–1406.
- (10) Mancuso, A.; Zhu, A.; Beardsley, N. J.; Glickson, J. D.; Wehrli, S.; Pickup, S. *Magn. Reson. Med.* **2005**, *54*, 67–78.
- (11) Aiken, N. R.; McGovern, K. A.; Ng, C. E.; Wehrle, J. P.; Glickson, J. D. *Magn. Reson. Med.* **1994**, *31*, 241–247.
- (12) Mancuso, A.; Beardsley, N. J.; Wehrli, S.; Pickup, S.; Matschinsky, F. M.; Glickson, J. D. *Biotechnol. Bioeng.* **2004**, *87*, 835–848.
- (13) Sriram, R.; Nguyen, J.; Santos, J. D.; Nguyen, L.; Sun, J.; Vigneron, S.; Van Criekinge, M.; Kurhanewicz, J.; MacKenzie, J. D. *Theranostics* **2018**, *8*, 3400–3407.
- (14) Keshari, K. R.; Sriram, R.; Van Criekinge, M.; Wilson, D. M.; Wang, Z. J.; Vigneron, D. B.; Peehl, D. M.; Kurhanewicz, J. *Prostate* **2013**, *73*, 1171–1181.
- (15) Chandrasekaran, P.; Seagle, C.; Rice, L.; Macdonald, J.; Gerber, D. A. *Tissue Engineering* **2006**, *12*, 2001–2008.
- (16) Mathiassen, T.; Høgh, A.; Karlsson, M.; Katsikis, S.; Wang, K.; Pennestri, M.; Ardenkjær-Larsen, J.; Jensen, P. *Journal of Magnetic Resonance Open* **2023**, *16–17*, No. 100131.
- (17) Monferrer, E.; Martín-Vañó, S.; Carretero, A.; García-Lizarribar, A.; Burgos-Panadero, R.; Navarro, S.; Samitier, J.; Noguera, R. *Sci. Rep.* **2020**, *10*, 6370.
- (18) Sutherland, R. *Science* **1988**, *240*, 177–184.
- (19) Xu, Q. *Frontiers in Bioengineering and Biotechnology* **2021**, *9*, 1–21.
- (20) Keshari, K. R.; Kurhanewicz, J.; Jeffries, R. E.; Wilson, D. M.; Dewar, B. J.; Van Criekinge, M.; Zierhut, M.; Vigneron, D. B.; Macdonald, J. M. *Magn. Reson. Med.* **2010**, *63*, 322–329.
- (21) Mancuso, A.; Pourfathi, M.; Kiefer, R. M.; Noji, M. C.; Siddiqui, S.; Profka, E.; Weber, C. N.; Pantel, A.; Kadlecsek, S. J.; Rizi, R.; Gade, T. P. *Metabolites* **2021**, *11*, 576.
- (22) Mangas Florencio, L.; Herrero Gómez, A. A DIY Bioreactor for in-situ Non-Invasive Metabolic Tracking in Bioengineered 3D Cell Models via Hyperpolarized <sup>13</sup>C NMR Spectroscopy. *CORA. Repositori de Dades de Recerca* **2024**.
- (23) Krishnan, V.; Murali, N. *Prog. Nucl. Magn. Reson. Spectrosc.* **2013**, *68*, 41–57.
- (24) Velasco-Mallorquí, F.; Rodríguez-Comas, J.; Ramón-Azcón, J. *Biofabrication* **2021**, *13*, 035044.
- (25) Herrero-Gómez, A.; Azagra, M.; Marco-Rius, I. *Biomedical Materials* **2022**, *17*, No. 045023.
- (26) Azagra, M.; Gomez-Cabeza, D.; Portela, A.; Matajusz, G.; Torras, N.; Martinez, E.; Marco-Rius, I. Leveraging Magnetic Resonance Imaging to Study Biocompatible Scaffolds Diffusion and Perfusion for Lab-on-a-Chip Systems. *ChemRxiv* **2024**.
- (27) Liang, J.; Susan Sun, X.; Yang, Z.; Cao, S. *Sci. Rep.* **2017**, *7*, 37626.
- (28) Jayawarna, V.; Richardson, S. M.; Hirst, A. R.; Hodson, N. W.; Saiani, A.; Gough, J. E.; Ulijn, R. V. *Acta biomaterialia* **2009**, *5*, 934–943.
- (29) Štampar, M.; Breznik, B.; Filipič, M.; Žegura, B. *Cells* **2020**, *9*, 2557.
- (30) Lees, H.; Millan, M.; Ahamed, F.; Eskandari, R.; Granlund, K. L.; Jeong, S.; Keshari, K. R. *NMR in biomedicine* **2021**, *34* (3), No. e4447.
- (31) Christensen, N. V.; Holm, R.; Sanchez, J. D.; Hansen, E. S. S.; Lerche, M. H.; Ardenkjær-Larsen, J. H.; Laustsen, C.; Bertelsen, L. B. *NMR in Biomedicine* **2024**, *37*, No. e5107.
- (32) Sriram, R.; Van Criekinge, M.; De Los Santos, J.; Ahamed, F.; Qin, H.; Nolley, R.; Delos Santos, R.; Tabatabai, Z. L.; Bok, R. A.; Keshari, K. R.; Vigneron, D. B.; Peehl, D. M.; Kurhanewicz, J. *Cancers* **2020**, *12*, 537.
- (33) Cacciamali, A.; Villa, R.; Dotti, S. *Frontiers in Physiology* **2022**, *13*, No. 836480.
- (34) Wesseler, M. F.; Taebnia, N.; Harrison, S.; Youhanna, S.; Preiss, L. C.; Kemas, A. M.; Vegvari, A.; Mokry, J.; Sullivan, G. J.; Lauschke, V. M.; et al. *Acta Biomaterialia* **2023**, *171*, 336–349.